

that any tendency for the induced squint itself to cause a visual impairment (strabismic amblyopia) in the deviating eye would actually reduce the likelihood of the nondeprived eye's continuing to dominate the cortex.

In six kittens (three MDB and three MDS), visual acuity in the previously deprived eye was determined daily by the jumping-stand method^{6,7}. Kittens were trained to discriminate between a vertical and a horizontal grating, the spatial frequency of which was increased in accordance with an ascending method of limits. The nondeprived eye was occluded when the previously deprived eye was tested. The visual acuity of the nondeprived eye was also determined during and after the recovery period, either directly or by measurement of the acuity with both eyes open⁶.

After at least 14 days of recovery, ocular dominance and orientation maps in the primary visual cortex of all ten kittens were obtained by optical imaging of intrinsic signals. For six kittens (three MDB, three MDS), both behavioural tests and optical imaging experiments were performed.

Optical imaging and analysis

Anaesthesia was induced with an intramuscular injection of ketamine (20–40 mg kg⁻¹) and xylazine (2–4 mg kg⁻¹). Animals were intubated and artificially ventilated (50–60% N₂O, 40–50% O₂, 0.9–1.2% halothane). Electrocardiogram, electroencephalogram, end-tidal CO₂ and rectal temperature were monitored continuously. Optical imaging of primary visual cortex was performed as described previously²⁵. Images were captured with either a cooled slow-scan charge-coupled device camera or an enhanced differential imaging system (ORA 2001 or Imager 2001; Optical Imaging Inc.), with the camera focused ~500 μm below the cortical surface. Visual stimuli, produced by a stimulus generator (VSG; Cambridge Research Systems), consisted of high-contrast, sinusoidally modulated gratings (0.2–0.6 cycle deg⁻¹) of four different orientations, drifting at a temporal frequency of 2 Hz, presented to the two eyes separately in randomized sequence, interleaved with trials in which the screen was blank. Single-condition responses (averages of 32–96 trials per eye and orientation) were divided (1) by responses to the blank screen, and (2) by the sum of responses to all four orientations ('cocktail blank')²⁵ to obtain iso-orientation maps. Signal amplitude was displayed on an eight-bit greyscale.

Ocular-dominance maps were obtained by dividing the sum of responses to all four orientations through one eye by the similar sum of responses through the other eye. Resulting maps were high-pass filtered (cutoff 1.3 mm). Within a region of interest that comprised the visually responsive part of the images, excluding blood vessel artefacts, pixels were assigned to the left and right eye, respectively, depending on whether their value was greater or less than 1.

Orientation preference maps were calculated by vectorial addition of four iso-orientation maps, and pseudo-colour coded. Orientation selectivity indices (OSIs) were calculated for responses at each pixel as

$$OSI = \frac{\sqrt{(R_0 - R_{90})^2 + (R_{45} - R_{135})^2}}{R_0 + R_{45} + R_{90} + R_{135}}$$

where R₀, R₄₅, R₉₀ and R₁₃₅ represent the responses in each of the four iso-orientation maps²⁶. OSI represents the magnitude of the orientation preference vector divided by the sum of all responses; it is therefore normalized to values between 0 and 1.

Electrophysiology

In one strabismic animal we determined quantitative orientation–direction tuning curves for 11 single units, recorded with glass-insulated tungsten microelectrodes and discriminated by their spike shapes (Brainware, Oxford, UK). All of these cells were dominated by the previously deprived eye. Responses to drifting gratings (optimum spatial and temporal frequency) of 16 different directions were averaged over five trials of 1.5 s duration. Smooth tuning curves were fitted to the data points on the basis of Fourier analysis²⁷, and preferred orientation and half-width of tuning at half-height were determined from these curves.

Received 9 April 2001; accepted 9 January 2002.

1. Wiesel, T. N. & Hubel, D. H. Comparison of the effects of unilateral and bilateral eye closure on cortical unit responses in kittens. *J. Neurophysiol.* **28**, 1029–1040 (1965).
2. Guillery, R. W. In *The Making of the Nervous System* (eds Parnevelas, J. G., Stern, C. J. & Sterling, R. V.) 356–379 (Oxford University Press, Oxford, 1988).
3. Mitchell, D. E. & Timney, B. in *Handbook of Physiology Section I (The Nervous System) Vol. 3 Part 1 (Sensory Processes)* (ed. Darian-Smith, I.) 507–555 (American Physiological Society, Bethesda, 1984).
4. Mitchell, D. E., Cynader, M. & Movshon, J. A. Recovery from the effects of monocular deprivation in kittens. *J. Comp. Neurol.* **176**, 53–64 (1977).
5. Mitchell, D. E. The extent of visual recovery from early monocular or binocular visual deprivation in kittens. *J. Physiol. (Lond.)* **395**, 639–660 (1988).
6. Giffin, F. & Mitchell, D. E. The rate of recovery of vision after early monocular deprivation in kittens. *J. Physiol. (Lond.)* **274**, 511–553 (1978).
7. Mitchell, D. E. & Gingras, G. Visual recovery after monocular deprivation is driven by absolute rather than relative visually-evoked activity levels. *Curr. Biol.* **8**, 1179–1182 (1998).
8. Hubel, D. H. & Wiesel, T. N. Binocular interaction in striate cortex of kittens reared with artificial squint. *J. Neurophysiol.* **28**, 1041–1059 (1965).
9. Crair, M. C., Ruthazer, E. S., Gillespie, D. C. & Stryker, M. P. Relationship between the ocular dominance and orientation maps in visual cortex of monocularly deprived cats. *Neuron* **2**, 307–318 (1997).
10. Sengpiel, F., Blakemore, C., Kind, P. C. & Harrad, R. Interocular suppression in the visual cortex of strabismic cats. *J. Neurosci.* **14**, 6855–6871 (1994).
11. Kiorpes, L., Kiper, D. C., O'Keefe, L. P., Cavanaugh, J. R. & Movshon, J. A. Neuronal correlates of amblyopia in the visual cortex of macaque monkeys with experimental strabismus and anisometropia. *J. Neurosci.* **18**, 6411–6424 (1998).

12. Murphy, K. M. & Mitchell, D. E. Bilateral amblyopia following a short period of reverse occlusion in kittens. *Nature* **323**, 536–538 (1986).
13. Blakemore, C. & Van Sluyters, R. C. Reversal of the physiological effects of monocular deprivation in the kitten: further evidence for a sensitive period. *J. Physiol. (Lond.)* **237**, 195–216 (1974).
14. Mitchell, D. E., Gingras, G. & Kind, P. C. Initial recovery of vision after early monocular deprivation in kittens is faster when both eyes are open. *Proc. Natl Acad. Sci. USA* **98**, 11662–11667 (2001).
15. Malach, R. & Van Sluyters, R. C. Strabismus does not prevent recovery from monocular deprivation: a challenge for simple Hebbian models of synaptic modification. *Vis. Neurosci.* **3**, 267–273 (1989).
16. Kirkwood, A., Lee, H.-K. & Bear, M. F. Co-regulation of long-term potentiation and experience-dependent synaptic plasticity in visual cortex by age and experience. *Nature* **375**, 328–331 (1995).
17. Blakemore, C., Vital-Durand, F. & Garey, L. J. Recovery from monocular deprivation in the monkey. I. Recovery of physiological effects in the visual cortex. *Proc. R. Soc. Lond. B* **213**, 399–423 (1981).
18. Blake, R., Crawford, M. L. & Hirsch, H. V. Consequences of alternating monocular deprivation on eye alignment and convergence in cats. *Invest. Ophthalmol.* **13**, 121–126 (1974).
19. Movshon, J. A. Reversal of the behavioural effects of monocular deprivation in the kitten. *J. Physiol. (Lond.)* **261**, 175–187 (1976).
20. Quick, M. W., Tigges, M., Gammon, J. A. & Boothe, R. G. Early abnormal visual experience induces strabismus in infant monkeys. *Invest. Ophthalmol. Vis. Sci.* **30**, 1012–1017 (1989).
21. Bienenstock, E. L., Cooper, L. N. & Munro, P. W. Theory for the development of neuron selectivity: orientation specificity and binocular interaction in visual cortex. *J. Neurosci.* **2**, 32–48 (1982).
22. Clothiaux, E. E., Bear, M. F. & Cooper, L. N. Synaptic plasticity in visual cortex: comparison of theory with experiment. *J. Neurophysiol.* **66**, 1785–1804 (1991).
23. Rittenhouse, C. D., Shouval, H. Z., Paradiso, M. A. & Bear, M. F. Monocular deprivation induces homosynaptic long-term depression in visual cortex. *Nature* **397**, 347–350 (1999).
24. Kind, P. C. Cortical plasticity: is it time for a change? *Curr. Biol.* **9**, R640–R643 (1999).
25. Bonhoeffer, T. & Grinvald, A. in *Brain Mapping: The Methods* (eds Toga, A. W. & Mazziotta, J. C.) 55–97 (Academic, London, 1996).
26. Bonhoeffer, T., Kim, D. S., Maloney, D., Shoham, D. & Grinvald, A. Optical imaging of the layout of functional domains in area 17 and across the area 17/18 border in cat visual cortex. *Eur. J. Neurosci.* **7**, 1973–1988 (1995).
27. Wörgötter, F. & Eysel, U. T. Quantitative determination of orientational and directional components in the response of visual cortical cells to moving stimuli. *Biol. Cybern.* **57**, 349–355 (1987).

Acknowledgements

We thank M. Bear and H. Shouval for their helpful discussions, and I. Kehrner and M. Jones for technical assistance. This work was supported by the Wellcome Trust (P.C.K.), the Medical Research Council (C.B., F.S., B.A.), Max-Planck-Gesellschaft (T.B., F.S.), the Canadian Institutes of Health Research (D.E.M.) and the Oxford McDonnell Centre for Cognitive Neuroscience (C.B., B.A.).

Competing interests statement

The authors declare that they have no competing financial interests.

Correspondence and requests for materials should be addressed to P.C.K. (e-mail: pkind@ed.ac.uk).

Spike-timing-dependent synaptic modification induced by natural spike trains

Robert C. Froemke & Yang Dan

Division of Neurobiology, Department of Molecular and Cell Biology, University of California, Berkeley, California 94720, USA

The strength of the connection between two neurons can be modified by activity, in a way that depends on the timing of neuronal firing on either side of the synapse^{1–10}. This spike-timing-dependent plasticity (STDP) has been studied by systematically varying the intervals between pre- and postsynaptic spikes. Here we studied how STDP operates in the context of more natural spike trains. We found that in visual cortical slices the contribution of each pre-/postsynaptic spike pair to synaptic modification depends not only on the interval between the pair, but also on the timing of preceding spikes. The efficacy of each spike in synaptic modification was suppressed by the preceding spike in the same neuron, occurring within several tens of

milliseconds. The direction and magnitude of synaptic modifications induced by spike patterns recorded *in vivo* in response to natural visual stimuli were well predicted by incorporating the suppressive inter-spike interaction within each neuron. Thus, activity-induced synaptic modification depends not only on the relative spike timing between the neurons, but also on the spiking pattern within each neuron. For natural spike trains, the timing of the first spike in each burst is dominant in synaptic modification.

Whole-cell recordings were made from pyramidal neurons in layer 2/3 (L2/3) of rat visual cortical slices to monitor excitatory postsynaptic potentials (EPSPs) evoked by extracellular stimulation applied in the same layer. To understand how complex spike trains induce synaptic modification, we first characterized the dependence of synaptic modification on the interval between the pre- and postsynaptic spikes, using a standard pairing protocol^{6,8-10}. Each pairing consisted of a single-pulse presynaptic stimulation and a brief postsynaptic depolarizing current injection that induced an action potential. After 60–80 pairings (0.2 Hz) at positive intervals

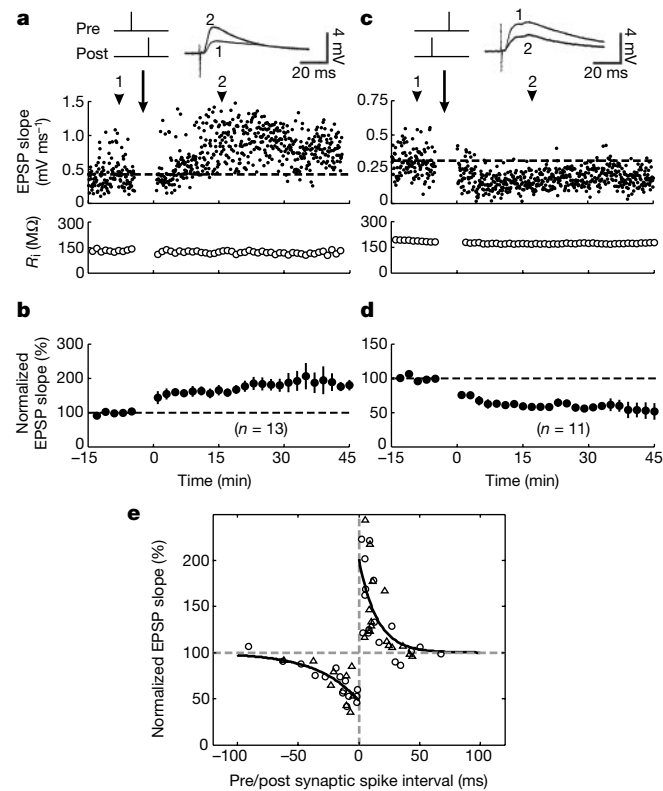


Figure 1 Synaptic modification of L2/3 visual cortical connections induced by pre-/postsynaptic spike pairs. **a**, Example of LTP (117%) induced by repetitive pre- and postsynaptic spiking at a positive interval (9.1 ms). Arrow, induction. Bottom, input resistance (R_i). **b**, Summary of effects of pre \rightarrow post spiking (increase of $62.5 \pm 12\%$, $n = 13$, $P < 0.001$, t -test; intervals: 2–15 ms). **c**, As in **a**, except LTD (–48%) was induced by a post \rightarrow pre spike pair (interval, –2 ms). **d**, Summary of effects of post \rightarrow pre spiking ($-41.5 \pm 4\%$, $n = 11$, $P < 0.0001$, intervals: –2 to –15 ms). **e**, Dependence of synaptic modification on pre/post inter-spike interval. Each point represents one experiment. Circles, normal ACSF ($A_+ = 103 \pm 10\%$, s.d., non-parametric bootstrap, $\tau_+ = 13.3 \pm 1.7$ ms, $n = 17$; $A_- = -51 \pm 1\%$, $\tau_- = 34.5 \pm 1.6$ ms, $n = 15$). Triangles, high divalent ACSF with bicuculline ($A_+ = 102 \pm 11\%$, $\tau_+ = 15.5 \pm 3.2$ ms, $n = 15$; $A_- = -52 \pm 6\%$, $\tau_- = 33.2 \pm 5.3$ ms, $n = 9$). No significant difference between parameters for the two solutions ($P > 0.5$). Curves, single-exponential, least-square fits of the combined data. Mean error of the fit, $18.2 \pm 2.1\%$. Correlation coefficient between the data and the fit, 0.88 . $R^2 = 1 - \frac{\sum e_i^2}{\sum y_i^2}$ (where e_i is the error, y_i is the measured effect of the i th experiment) = 0.72.

(pre \rightarrow post) of 2 to 15 ms, we observed long-term potentiation (LTP) (Fig. 1a, b). The same number of pairings at negative intervals (post \rightarrow pre, –2 to –15 ms), however, induced long-term depression (LTD) (Fig. 1c, d). Figure 1e summarizes the observed synaptic modification as a function of the pre/post inter-spike interval. Synaptic potentiation was observed at intervals between 0 and 20 ms, whereas depression was observed between 0 and –40 ms, comparable to the temporal window for STDP found at several other glutamatergic excitatory synapses^{5,6,8-9}. Similar LTP and LTD windows were also observed in experiments performed in high divalent external solution containing 4 mM Mg^{2+} , 4 mM Ca^{2+} (to reduce polysynaptic transmission), and 3 μM bicuculline (antagonist of the GABA_A receptor) (Fig. 1e, triangles). Thus the observed STDP is independent of polysynaptic transmission and cortical inhibition. To obtain a quantitative description of the temporal window, we fitted the data on each side with an exponential function $\Delta w = Ae^{-|\Delta t|/\tau}$, where Δw is the percentage change in synaptic strength, A and τ are the scaling factor and time constant of the exponential function, respectively, and Δt is the pre/post inter-spike interval. A and τ were found to be 101% and 14.8 ms respectively for potentiation, and –52% and 33.8 ms for depression.

To predict the effect of a pair of complex spike trains in synaptic modification, a straightforward approach is to combine the contri-

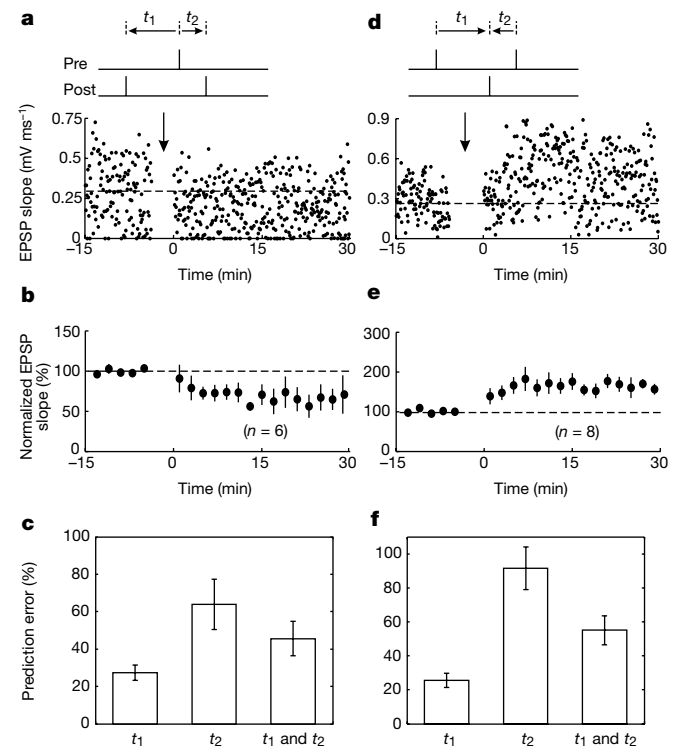


Figure 2 Synaptic modification induced by spike triplets. **a**, Example of LTD induced by a ‘1/2’ triplet. Pre/post spike pair interval defined as $t_2^{post} - t_1^{pre}$. Right arrows, positive; left arrows, negative. **b**, Summary of ‘1/2’ experiments satisfying: (1) $t_1 < 0$, (2) $t_2 > 0$, (3) $|t_1 - t_2| \leq 30$ ms, and (4) prediction of the independent model was potentiation or no change. The measured effect was depression ($-33 \pm 11\%$, $n = 6$, $P < 0.05$). **c**, Mean prediction errors based on t_1 , t_2 , and t_1 and t_2 combined (using the independent model) for all the ‘1/2’ triplets such that both $|t_1|$ and $|t_2| < 15$ ms ($n = 11$). Error bars, \pm s.e.m. **d**, As in **a**, except LTP was induced by a ‘2/1’ triplet. **e**, Summary of ‘2/1’ triplet experiments satisfying: (1) $t_1 > 0$, (2) $t_2 < 0$, (3) $|t_1 - t_2| \leq 30$ ms, and (4) prediction of the independent model was depression or no change. The measured effect was potentiation ($65.0 \pm 17\%$, $n = 8$, $P < 0.01$). **f**, Mean prediction errors based on t_1 , t_2 , and t_1 and t_2 combined (using the independent model) for all ‘2/1’ triplets such that both $|t_1|$, $|t_2| < 15$ ms ($n = 14$). Prediction error based on t_1 was smaller than that based on t_2 ($P < 0.001$) and t_1 and t_2 combined ($P < 0.005$).

butions of all pre/post spike pairs in the two spike trains^{11–13}. However, the contribution of each pre/post spike pair may depend not only on its interval, as shown in Fig. 1e, but also on the presence of other spikes in both neurons in an unknown manner. Thus we carried out a series of experiments, using spike patterns of increasing complexity, to examine whether the contribution of each pre/post spike pair depends on the presence of other spikes in the pre- and postsynaptic cells and to develop a quantitative method for estimating the effects of complex spike trains on synaptic strength.

We first added a third spike either pre- or postsynaptically to form a 'triplet', each repeated 60–80 times at 0.2 Hz to induce synaptic modification. A typical experiment using a '1/2' triplet (1 pre and 2 post) is shown in Fig. 2a. According to the temporal window measured with isolated pre/post spike pairs (Fig. 1e), the first post → pre spike pair (spike time, $t_1 = -24$ ms) was expected to reduce the synaptic strength by 26%, and the following pre → post spike pair ($t_2 = 6$ ms) should increase the strength by 67%. Assuming that the two spike pairs contribute independently to synaptic modification and that the contributions are combined multiplicatively (see Methods), this triplet should induce a 24% synaptic potentiation. However, we observed a clear reduction (32%) of synaptic strength. Similar results were obtained in all six experiments using such triplets (Fig. 2b). To characterize the contribution of each spike pair in synaptic modification, we further measured the effects of '1/2' triplets over a range of t_1 and t_2 values ($n = 25$), and compared the results with the predicted synaptic modification based on t_1 , t_2 , or t_1 and t_2 combined (assuming independent contributions of the two spike pairs). We found that when the three spikes were in close proximity (both $|t_1|$ and $|t_2| < 15$ ms), the prediction based on t_1 was significantly better than that based on t_2 (Fig. 2c, $P < 0.01$, Student's paired t -test), indicating that the first spike pair played a dominant role in synaptic modification. Moreover, the prediction based on t_1 was also better than that based on t_1 and t_2 combined (Fig. 2c). This further indicated that the two spike pairs did not contribute independently to synaptic modification, and the contribution of the second pair was strongly suppressed by the presence of the preceding postsynaptic spike. This suppressive effect, however, depended on the proximity of the preceding spike. For $t_1 < -30$ ms, the synaptic modification induced by the triplet could be largely predicted by t_2 (see Fig. 3b).

In a complementary series of experiments, we measured the effects of '2/1' triplets (2 pre, 1 post) to determine whether the contribution of a pre/post spike pair can also be affected by a preceding presynaptic spike. In the example shown in Fig. 2d, the first pre → post spike pair ($t_1 = 6.5$ ms) should induce a 65% potentiation, whereas the following post → pre spike pair ($t_2 = -0.5$ ms) should cause a 52% reduction of synaptic strength. Assuming independent contributions of the two spike pairs (combined multiplicatively), the expected effect of the triplet is a 20% reduction of synaptic strength. The observed effect, however, was a strong synaptic potentiation of 85%. Similar results were obtained in all eight experiments using such triplets (Fig. 2e), again indicating a dominant contribution of the first spike pair. When both t_1 and t_2 were within ± 15 ms, the effect of the triplet was best predicted by t_1 (Fig. 2f). For $t_1 > 30$ ms, however, the synaptic modification induced by the triplet could be largely predicted by t_2 (see Fig. 3b). Thus, a preceding spike in the presynaptic neuron can also suppress the contribution of a pre/post spike pair in synaptic modification.

On the basis of the above observations we proposed a simple model for the inter-spike interactions in synaptic modification. The contribution of each pre/post spike pair depends not only on the interval between the pair (Fig. 1e), but also on the spike 'efficacy', which is suppressed by the preceding spike in each neuron. The spike efficacy is reduced to zero immediately after the preceding spike, and recovers exponentially towards one (Fig. 3a). By fitting

the data of '2/1' triplets ($n = 28$), the time constant of suppression between consecutive presynaptic spikes was found to be 34 ms. Similarly, from the data of '1/2' triplets ($n = 25$), the time constant of suppression in the postsynaptic neuron was found to be 75 ms. To evaluate the validity of the suppression model in accounting for the effects of spike triplets, we compared the predicted and measured effects of both '1/2' and '2/1' triplets within a window of ± 100 ms for t_1 and t_2 . We found that the model correctly predicted the

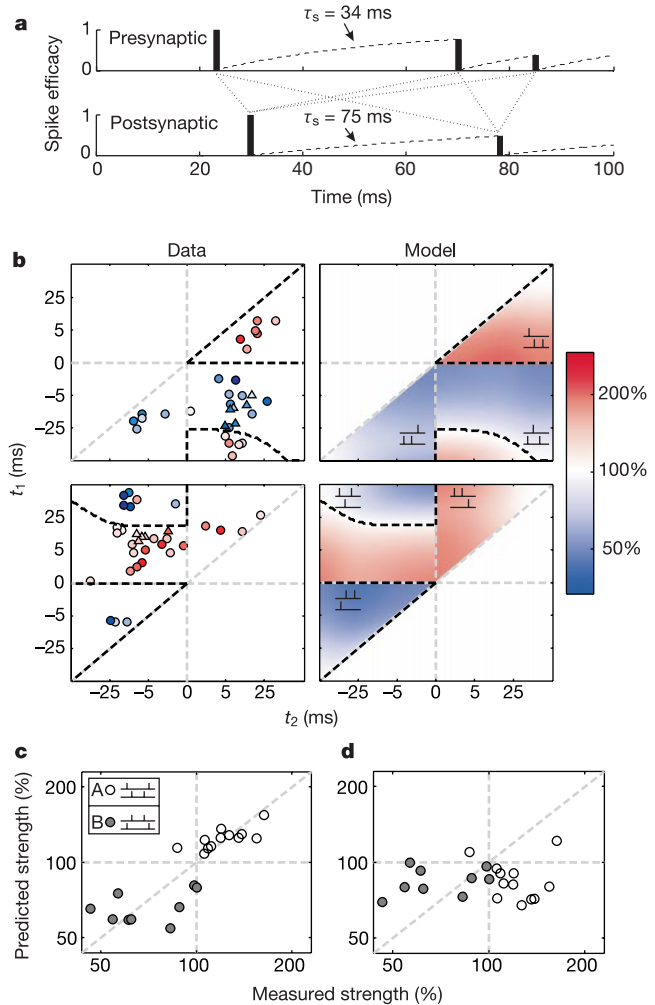


Figure 3 Suppressive interaction between consecutive spikes for triplets and quadruplets. **a**, Model of inter-spike suppression in pre- and postsynaptic cells. Vertical lines indicate spikes, with height indicating efficacy. Dashed curves, efficacy as a function of time. Dotted lines, pre/post spike pairs. **b**, Comparison between measured (Data) and predicted (Model) synaptic modification induced by '1/2' (top) and '2/1' triplets (bottom). Circles, normal ACSF; triangles, high divalent ACSF with bicuculline; each symbol represents one experiment. Dashed lines, borders between predicted potentiation and depression regions. Scale, degree of synaptic modification (red, potentiation; blue, depression). Suppression model: correlation coefficients between predicted and measured effects are 0.89 for '1/2', 0.76 for '2/1' triplets; R^2 is 0.78 for '1/2', 0.59 for '2/1' triplets. Independent model: correlation coefficients are 0.74 for '1/2', 0.55 for '2/1' triplets; R^2 is 0.19 for '1/2', 0.02 for '2/1' triplets. **c**, Predicted versus measured effects of spike quadruplets, based on the suppression model. Open symbols, type A, pre → post → post → pre ($n = 12$, intervals: pre → post, 8.8 ± 2.0 ms, s.d.; post → pre, -9.6 ± 5.2 ms; post → post, $10.6-181.8$ ms). Filled symbols, type B, post → pre → pre → post ($n = 9$, intervals: pre → post, 9.0 ± 6.0 ms; post → pre, -7.9 ± 2.3 ms; pre → pre, $9.6-102.5$ ms). Mean prediction error, $14.6 \pm 2.6\%$; correlation coefficient, 0.85; R^2 , 0.72. **d**, As in **c**, except predictions are based on the independent model. Mean prediction error, $33.7 \pm 4.5\%$, larger than the suppression model ($P < 0.005$); correlation coefficient, 0.06; R^2 , -0.24 .

direction of synaptic modification in 50/53 triplet experiments (Fig. 3b), suggesting that the suppression model with only two free parameters provides a good description of synaptic modification induced by spike triplets.

In principle, the inter-spike suppression may be mediated by the inhibitory synaptic interactions in the local cortical circuitry¹⁴. However, significant suppression was also observed in both '1/2' and '2/1' triplet experiments in high divalent solution containing bicuculline (Fig. 3b, triangles), indicating that the suppression is mediated by mechanisms in the pre- or postsynaptic neurons rather than by the polysynaptic cortical circuitry. Consistent with previous studies^{15,16}, we noticed significant paired-pulse depression at these intracortical synapses (data not shown), suggesting that the suppression between presynaptic spikes during synaptic modification may result from short-term depression of transmitter release¹⁷ or desensitization/saturation of postsynaptic glutamate receptors¹⁸. The suppression between postsynaptic spikes, on the other hand, may be due to Ca^{2+} -dependent conductances¹⁹ or downstream mechanisms involved in activity-dependent synaptic modification^{20,21}. When more quantitative information concerning these processes becomes available, detailed biophysical models^{22,23} may be constructed to describe the inter-spike interactions observed here. In the following experiments we examined whether the simple suppression model derived from the triplet experiments provides a useful description of the effects of complex spike patterns in synaptic modification.

To extend the complexity of the spike pattern, we next added another spike to form 'quadruplets' (2 pre, 2 post), with the spike sequence being either pre → post → post → pre (type A) or post → pre → pre → post (type B) (Fig. 3c, inset). These patterns con-

tained two pre/post spike pairs with positive intervals and two pairs with negative intervals, and the measured effects of these quadruplets provide a direct test of the inter-spike suppression within each neuron. According to the suppression model, as the first spike of each neuron plays a dominant role in determining the sign and magnitude of synaptic modification, the type-A quadruplets are likely to induce potentiation whereas type-B quadruplets are likely to induce depression. However, without suppression the two types of quadruplets should have similar effects. As shown in Fig. 3c, the measured effects of the two types of quadruplets were clearly different, with type A (open circles) inducing mostly potentiation and type B inducing depression (filled circles). The measured effects agreed well with the suppression model, but were inconsistent with the prediction based on independent contributions of the spike pairs (Fig. 3d).

Finally, we examined synaptic modification in cortical slices induced by natural spike patterns occurring *in vivo* in response to visual stimuli. Spike trains were recorded simultaneously from neighbouring V1 neurons of the anaesthetized cat in response to time-varying natural scenes (Fig. 4a). Segments of spike trains (1 s, containing 6–12 spikes) from two neurons with partially overlapping receptive fields were applied to pre- and postsynaptic neurons in the slice to induce synaptic modification. Figure 4b shows three examples of these spike train segments, each of which induced a significant long-term synaptic modification after 60 repetitions (0.2 Hz). Figure 4c summarizes the results of 22 experiments using different pairs of natural spike train segments. We found that the observed synaptic modification agreed well with that predicted by the suppression model. In contrast, the data fit poorly with the prediction based on independent contributions of all spike

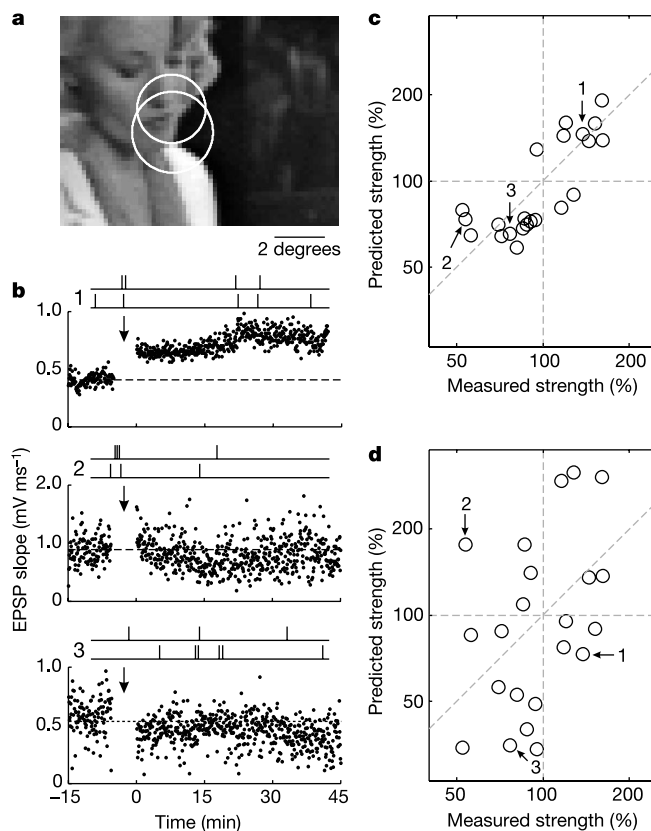


Figure 4 Synaptic modification induced by natural spike-train segments. **a**, Frame (64 × 48 pixels, 0.17° per pixel) in a movie used to evoke cortical responses in the cat. Circles, receptive fields. **b**, Examples of synaptic modification induced by pairs of natural spike-train segments (1 s). Synaptic modification: top, 37%; middle, -47%; bottom, -23%. **c**, Predicted versus measured effect, based on the suppression model. Arrows,

experiments in **b**. Mean prediction error, $20.7 \pm 2.4\%$ (s.e.m., $n = 22$); correlation coefficient, 0.79; R^2 , 0.53. **d**, As in **c**, but predictions are based on the independent model. Mean prediction error, $54.8 \pm 6.6\%$, larger than the suppression model ($P < 0.0001$); correlation coefficient: 0.42; R^2 , -2.33.

pairs (Fig. 4d). Thus, the dependence on the pre/post inter-spike interval (Fig. 1e) and the suppressive interaction between consecutive spikes within each neuron (Fig. 3) together provide a good description of STDP induced by complex spike patterns encountered *in vivo*.

Spike-timing-dependent modification of excitatory connections between L2/3 neurons is likely to play an important role in plasticity of visual cortical circuitry *in vivo*. Recent studies have shown that timing of visual stimuli on the order of 20 ms can affect the direction and magnitude of plasticity in orientation tuning of adult cortical neurons²⁴, and such functional plasticity may be mediated by STDP of excitatory intracortical connections. A direct implication of the inter-spike suppression shown here is that timing of the first spike in each burst has a crucial role in determining the sign and magnitude of synaptic modification. In many cortical neurons, stimulus onset or saccadic eye movement evokes fast initial transients followed by sustained responses, and our results suggest that timing of the initial transients may be especially important for long-term synaptic modification. Previous studies have shown that presynaptic spike timing in complex spike trains is important in neural signalling owing to short-term synaptic plasticity^{15,16,25}. Studies of STDP have also underscored the critical role of precise spike timing in long-term synaptic modification^{3–10}. Our results show that the spike timing dependence of long-term synaptic modification induced by complex spike trains must include not only the relative timing between pre- and postsynaptic spiking, but also the inter-spike intervals within each neuron. □

Methods

Visual cortical slice preparation

Acute visual cortical slices were prepared from 2–5-week-old Sprague–Dawley rats (no correlation between age and synaptic modification; LTP: $r = 0.09$, $P > 0.4$, $n = 67$; LTD: $r = -0.16$, $P > 0.2$, $n = 62$; analysis of variance, ANOVA). Rats were deeply anaesthetized with halothane, decapitated, and the brain quickly placed into ice-cold dissection buffer containing (in mM): 206 sucrose, 2 KCl, 2 MgSO₄, 1.25 NaH₂PO₄, 1 CaCl₂, 1 MgCl₂, 26 NaCHO₃, and 10 dextrose, bubbled with 95% O₂/5% CO₂ (pH 7.4). Coronal visual cortical slices (300–400 μm thick) were prepared with a vibratome (Pelco), placed in warm dissection buffer (33–35°C) for <30 min, transferred to a holding chamber containing artificial cerebrospinal fluid (ACSF, in mM: 124 NaCl, 2 KCl, 1.5 MgSO₄, 1.25 NaH₂PO₄, 2.5 CaCl₂, 26 NaCHO₃ and 10 dextrose), and kept at 22–24°C for >1 h before use. For experiments, slices were transferred to the recording chamber and perfused (4.0–4.5 ml min⁻¹) with oxygenated ACSF at 22–24°C. Some specified experiments were performed in modified ACSF containing 4 mM CaCl₂, 4 mM MgSO₄, and 3 μM bicuculline methiodide. Several experiments performed at higher temperature (35.8 ± 1.5°C) confirmed the dependence of synaptic modification on both the pre/post and inter-spike intervals within each neuron (data not shown).

Electrophysiology

Somatic whole-cell recordings were made in current-clamp with an Axopatch 200B amplifier (Axon) using infrared differential interference optics (IR-DIC) video microscopy. L2/3 pyramidal cells were selected on morphology and regular spiking in response to current injection²⁶. Patch pipettes (3–7 MΩ) were filled with intracellular solution (in mM: 120 K-gluconate, 10 HEPES, 0.1 EGTA, 20 KCl, 2 MgCl₂, 10 phosphocreatine, 2 ATP, and 0.25 GTP). The mean resting potential was -71.1 ± 0.8 mV, corrected for the measured liquid junction potential (6.8 mV). The series resistance was 13.3 ± 0.8 MΩ. R_i (153.2 ± 7.8 MΩ) was monitored with hyperpolarizing current pulses (50 pA, 100 ms); cells were excluded if input resistance R_i changed >30% over the entire experiment. Data were filtered at 2 kHz, digitized at 10 kHz, and analysed with Clampfit 8 (Axon). Extracellular stimulation (0.1–1 ms, 5–150 μA) was applied in L2/3 with a small glass bipolar electrode 0.05–1.0 mm from the recording electrode. EPSP size: 3.2 ± 2.8 mV (s.d., $n = 100$). The initial slope of EPSP (first 2 ms) was used to calculate synaptic strength, as this component reflects monosynaptic input^{8,10}. To ensure L2/3 pathway specificity, we placed a second stimulating electrode in L4 in the same column and monitored the evoked EPSPs. During induction, L4 stimulation was temporarily interrupted. In experiments where synaptic modification was induced in L2/3, the L4 EPSPs were unaffected, indicating independence of L2/3 and L4 stimulation. Stable baselines of synaptic strength were established by 6–12 min of stimulation at 0.2 Hz. Synaptic strength after induction was measured 11–20 min after the end of the induction protocol. During induction, postsynaptic spiking was evoked with depolarizing current pulses (1 nA, 2–3 ms). Presynaptic spike timing was defined as the onset of EPSP and postsynaptic spike timing was measured at the peak of the action potential^{5,6,8}. To collect natural spike patterns, natural scene movies were used as visual stimuli, and extracellular recordings were made in cat visual cortex^{24,27}. Spike train segments for slice experiments were sampled from five simultaneously recorded cell pairs.

Predicting the effects of spike train segments

To predict the effects of spike train segments using the suppression model, each pre- and postsynaptic spike was assigned an efficacy, which depends only on the interval from the preceding spike in the same neuron: $\epsilon_i = 1 - e^{-(t_i - t_{i-1})/\tau_s}$, where ϵ_i is the efficacy of the *i*th spike, t_i and t_{i-1} are the timings of the *i*th and (*i* - 1)th spike, respectively, and τ_s is the suppression time constant. The contribution of each pre/post spike pair to synaptic modification was estimated as $\Delta w_{ij} = \epsilon_i^{pre} \epsilon_j^{post} F(\Delta t_{ij})$, where Δw_{ij} is the synaptic modification due to the *i*th presynaptic spike and the *j*th postsynaptic spike, ϵ_i^{pre} and ϵ_j^{post} are the efficacies of the two spikes, respectively, and Δt_{ij} is the interval between the two spikes, $t_j^{post} - t_i^{pre}$. The function *F* represents the temporal window for STDP measured with isolated spike pairs (Fig. 1e), expressed as:

$$F(\Delta t) = \begin{cases} A_+ e^{-|\Delta t|/\tau_+} & \text{if } \Delta t > 0 \\ A_- e^{-|\Delta t|/\tau_-} & \text{if } \Delta t < 0 \end{cases}$$

where *A* is the scaling factor, τ is the time constant, + means LTP and - means LTD. The net effect of spike train segment pairs was estimated by combining the contributions of all spike pairs multiplicatively²⁸: $1 + \Delta w = \prod_{ij}(1 + \Delta w_{ij})$. Suppression time constants for the pre- and postsynaptic neurons, τ_s^{pre} (34 ms) and τ_s^{post} (75 ms), were determined from the '2/1' and '1/2' triplet experiments, respectively, chosen to minimize mean prediction error: |predicted effect - measured effect|. To predict the effects using the independent model, ϵ^{pre} and ϵ^{post} were set to one regardless of the inter-spike interval.

Alternatively, the contributions of different spike pairs can be combined additively^{11–13,28}: $\Delta w = \sum_{ij} \Delta w_{ij}$. Under the additive model, $\tau_s^{pre} = 28$ ms, $\tau_s^{post} = 88$ ms. For quadruplet experiments, the mean prediction errors were 16.1 ± 3.0% (s.e.m.) (suppression model) and 29.4 ± 5.7% (independent model). For natural spike train segments, mean prediction errors were 19.5 ± 2.5% (suppression model) and 45.5 ± 9.3% (independent model). These errors were not significantly different from those of the multiplicative model (see legends of Figs 3c, 3d and 4c, 4d; $P > 0.25$, *t*-test).

Received 17 December 2001; accepted 15 January 2002.

1. Levy, W. B. & Steward, O. Temporal contiguity requirements for long-term associative potentiation/depression in the hippocampus. *Neuroscience* **8**, 791–797 (1983).
2. Gustafsson, B., Wigstrom, H., Abraham, W. C. & Huang, Y. Y. Long-term potentiation in the hippocampus using depolarizing current pulses as the conditioning stimulus to single volley synaptic potentials. *J. Neurosci.* **7**, 774–780 (1987).
3. Markram, H., Lubke, J., Frotscher, M. & Sakmann, B. Regulation of synaptic efficacy by coincidence of postsynaptic APs and EPSPs. *Science* **275**, 213–215 (1997).
4. Debanne, D., Gahwiler, B. H. & Thompson, S. M. Long-term synaptic plasticity between pairs of individual CA3 pyramidal cells in rat hippocampal slice cultures. *J. Physiol. (Lond)* **507**, 237–247 (1998).
5. Zhang, L. I., Tao, H. W., Holt, C. E., Harris, W. A. & Poo, M. A critical window for cooperation and competition among developing retinotectal synapses. *Nature* **395**, 37–44 (1998).
6. Bi, G. Q. & Poo, M. M. Synaptic modifications in cultured hippocampal neurons: dependence on spike timing, synaptic strength, and postsynaptic cell type. *J. Neurosci.* **18**, 10464–10472 (1998).
7. Egger, V., Feldmeyer, D. & Sakmann, B. Coincidence detection and changes of synaptic efficacy in spiny stellate neurons in rat barrel cortex. *Nature Neurosci.* **2**, 1098–1105 (1999).
8. Feldman, D. E. Timing-based LTP and LTD at vertical inputs to layer II/III pyramidal cells in rat barrel cortex. *Neuron* **27**, 45–56 (2000).
9. Nishiyama, M., Hong, K., Mikoshiba, K., Poo, M. M. & Kato, K. Calcium stores regulate the polarity and input specificity of synaptic modification. *Nature* **408**, 584–588 (2000).
10. Boettiger, C. A. & Doupe, A. J. Developmentally restricted synaptic plasticity in a songbird nucleus required for song learning. *Neuron* **31**, 809–818 (2001).
11. Kempter, R., Gerstner, W. & van Hemmen, J. L. Hebbian learning and spiking neurons. *Phys. Rev. E* **59**, 4498–4514 (1999).
12. Roberts, P. D. Computational consequences of temporally asymmetric learning rules: I. Differential hebbian learning. *J. Comput. Neurosci.* **7**, 235–246 (1999).
13. Song, S., Miller, K. D. & Abbot, L. F. Competitive Hebbian learning through spike-timing-dependent synaptic plasticity. *Nature Neurosci.* **3**, 919–926 (2000).
14. Somogyi, P., Tamas, G., Lujan, R. & Buhl, E. H. Salient features of synaptic organisation in the cerebral cortex. *Brain Res. Rev.* **26**, 113–135 (1998).
15. Tsodyks, M. V. & Markram, H. The neural code between neocortical pyramidal neurons depends on neurotransmitter release probability. *Proc. Natl Acad. Sci. USA* **94**, 719–723 (1997).
16. Varela, J. A. et al. A quantitative description of short-term plasticity at excitatory synapses in layer II/III of rat primary visual cortex. *J. Neurosci.* **17**, 7926–7940 (1997).
17. Zucker, R. S. Calcium- and activity-dependent synaptic plasticity. *Curr. Opin. Neurobiol.* **9**, 305–313 (1999).
18. Zorumski, C. F. & Thio, L. L. Properties of vertebrate glutamate receptors: calcium mobilization and desensitization. *Prog. Neurobiol.* **39**, 295–336 (1992).
19. Stuart, G. J. & Sakmann, B. Active propagation of somatic action potentials into neocortical pyramidal cell dendrites. *Nature* **367**, 69–72 (1994).
20. Malenka, R. C. & Nicoll, R. A. Long-term potentiation—a decade of progress? *Science* **285**, 1870–1874 (1999).
21. Lisman, J. E. & Zhabotinsky, A. M. A model of synaptic memory: a CaMKII/PP1 switch that potentiates transmission by organizing an AMPA receptor anchoring assembly. *Neuron* **31**, 191–201 (2001).
22. Senn, W., Markram, H. & Tsodyks, M. An algorithm for modifying neurotransmitter release probability based on pre- and postsynaptic spike timing. *Neural Comput.* **13**, 35–67 (2001).
23. Rao, R. P. & Sejnowski, T. J. Spike-timing-dependent hebbian plasticity as temporal difference learning. *Neural Comput.* **13**, 2221–2237 (2001).
24. Yao, H. & Dan, Y. Stimulus timing-dependent plasticity in cortical processing of orientation. *Neuron* **32**, 315–323 (2001).
25. Dobrunz, L. E. & Stevens, C. F. Response of hippocampal synapses to natural stimulation patterns. *Neuron* **22**, 157–166 (1999).

26. Connors, B. W. & Gutnick, M. J. Intrinsic firing patterns of diverse neocortical neurons. *Trends Neurosci.* **13**, 99–104 (1990).
27. Stanley, G. B., Li, F. F. & Dan, Y. Reconstruction of natural scenes from ensemble response in the lateral geniculate nucleus. *J. Neurosci.* **19**, 8036–8042 (1999).
28. van Rossum, M. C., Bi, G. Q. & Turrigiano, G. G. Stable Hebbian learning from spike timing-dependent plasticity. *J. Neurosci.* **20**, 8812–8821 (2000).

Acknowledgements

We thank K. Djupsund for help in recording natural spike trains, and J. Long, M. Frerking and R. S. Zucker for discussions. This work was supported by grants from the National Science Foundation and National Eye Institute. R.C.F. is a recipient of the Howard Hughes Predoctoral Fellowship.

Competing interests statement

The authors declare that they have no competing financial interests.

Correspondence and requests for materials should be addressed to Y.D. (e-mail: ydan@uclink4.berkeley.edu).

Rac function and regulation during *Drosophila* development

Satoko Hakeda-Suzuki*, Julian Ng†, Julia Tzu†, Georg Dietzl*, Yan Sun*, Matthew Harms†, Tim Nardine†, Liqun Luo†‡ & Barry J. Dickson*

* Research Institute of Molecular Pathology, Dr. Bohr-Gasse 7, A-1030 Vienna, Austria

† Department of Biological Sciences, and ‡ Neurosciences Program, Stanford University, Stanford, California 94035, USA

Rac GTPases regulate the actin cytoskeleton to control changes in cell shape^{1,2}. To date, the analysis of Rac function during development has relied heavily on the use of dominant mutant isoforms. Here, we use loss-of-function mutations to show that the three *Drosophila* Rac genes, *Rac1*, *Rac2* and *Mtl*, have overlapping functions in the control of epithelial morphogenesis, myoblast fusion, and axon growth and guidance. They are not required for the establishment of planar cell polarity, as had been suggested on the basis of studies using dominant mutant isoforms^{3,4}. The guanine nucleotide exchange factor, Trio, is essential for Rac function in axon growth and guidance, but not for epithelial morphogenesis or myoblast fusion. Different Rac activators thus act in different developmental processes. The specific cellular response to Rac activation may be determined more by the upstream activator than the specific Rac protein involved.

In *Drosophila*, studies using constitutively active and dominant negative mutants have implicated Rac1 in closure of the dorsal epidermis⁵, myoblast fusion⁶, the establishment of planar cell polarity^{3,4}, and the control of axon growth⁶ and guidance⁷. Each of these processes requires dynamic remodelling of the actin cytoskeleton, although the extracellular signals and the cellular responses involved seem to be different in each case. Given the ability of dominant mutant Rac proteins to interfere with cytoskeletal dynamics¹, it is not surprising to find that they perturb each of these processes. But are endogenous Rac proteins actually required for these processes, and if so, which proteins are involved, and how are they regulated? These questions cannot be answered using dominant mutant proteins. They require the phenotypic analysis of loss-of-function mutations in each of the endogenous Rac genes.

The *Drosophila* genome contains two highly similar Rac genes, *Rac1* and *Rac2* (refs 5, 6, 8, 9). A third gene, *Mtl*, encodes a closely

related GTPase that is structurally similar to both Rac and Cdc42 GTPases¹⁰, but functionally (as we now show) behaves like Rac1 and Rac2. We therefore refer to *Rac1*, *Rac2* and *Mtl* collectively as the *Drosophila* Rac genes (Fig. 1a). All three genes are ubiquitously expressed during development^{5,6,8,10}. The isolation of loss-of-function *Rac1* and *Rac2* mutations is described in the accompanying paper¹¹. A loss-of-function mutation in the *Mtl* gene was generated by imprecise excision of a P-element inserted in the first non-coding exon. We recovered a 2,068-base pair (bp) deletion that removes the entire *Mtl* open reading frame, but no part of any other predicted gene (Fig. 1b). Animals homozygous for this deletion, *Mtl*^Δ, as well as both *Rac1* and *Rac2* single mutants¹¹, are viable and fertile. The *Rac2 Mtl* double mutant is also viable and fertile. All other combinations are homozygous lethal.

We used these loss-of-function mutations to assess the contribution of each Rac protein to a set of distinct cell-shape changes that occur during *Drosophila* development. We examined embryos lacking both the maternal and zygotic contributions of one or more Rac gene, and also pupae and adults that were homozygous mutant either entirely or in large clones of cells. For pupae and adults, we used both the strong hypomorph *Rac1*^{J10} and the null allele *Rac1*^{J11}, together with the null deletion alleles for *Rac2* and *Mtl* (*Rac2*^Δ and *Mtl*^Δ). Analyses in the embryo were restricted to the use of the *Rac1*^{J10} allele, as triple mutant embryos could not be recovered using the null allele *Rac1*^{J11}. Evidently, Rac proteins also have important but still uncharacterized functions during oogenesis and early embryogenesis.

During *Drosophila* embryogenesis, opposing lateral epidermal sheets move towards one another, meeting and fusing seamlessly at the dorsal midline. This process of dorsal closure resembles ventral enclosure in *Caenorhabditis elegans*¹²; and wound healing in vertebrates¹³. It is believed to be driven, at least in part, by an actomyosin contractile ring that assembles at the leading edge^{14,15}, with lamellipodial and filopodial protrusions facilitating adhesion and alignment as the epidermis is sealed¹⁶. Expression of dominant negative Rac1 in epidermal cells prevents formation of the actomyosin cable and completion of dorsal closure⁵, suggesting that at least one endogenous Rac protein might be involved. We determined that all three Rac proteins contribute to dorsal closure (Fig. 1c–g). Triple mutant Rac embryos fail to complete dorsal closure (Fig. 1c, e). Little or no actin accumulation is seen at the leading epidermal edge, and both lamellipodia and filopodia are lacking (Fig. 1g). The underlying amnioserosa cells appear normal. Weaker and less frequent defects are also seen in *Rac1 Rac2* and *Rac1 Mtl* double mutant embryos (Fig. 1c). All remaining single and double mutant embryos successfully complete dorsal closure (Fig. 1c). Dorsal closure thus relies more on Rac1 than either Rac2 or Mtl, although any one of the three is largely sufficient.

Quite different cell-shape changes occur during cell fusion, a striking example of which is the fusion of myoblasts to form multinucleate muscle fibres¹⁷. The role of the actin cytoskeleton in myoblast fusion remains unclear. Most likely, it is involved in the formation of a vesicular prefusion complex that assembles at the apposed plasma membranes¹⁸. Expression of either dominant negative or dominant active Rac1 in *Drosophila* myoblasts blocks their fusion⁶, but here too the precise roles and contributions of individual Rac genes are unknown. We found that little or no myoblast fusion occurs in either *Rac1 Rac2* double mutant (Fig. 1j) or *Rac1 Rac2 Mtl* triple mutant embryos. In contrast, myoblast fusion appears to be complete in *Rac1* and *Mtl* single and double mutants, whereas only a few isolated myoblasts fail to fuse in *Rac2* single mutants and *Rac2 Mtl* double mutants (Fig. 1i). Myoblast fusion thus requires either Rac1 or Rac2, but not Mtl.

Actin rearrangements also underlie the establishment of planar cell polarity (PCP) within an epithelium¹⁹. In *Drosophila*, PCP has been studied most extensively in the context of eye and wing development. Photoreceptors in the eye are arranged in a trapezoi-